JOURNAL OF MATERIALS SCIENCE 22 (1987) 2867–2880

The formation of G-phase in 20/25 Nb stainless steel AGR fuel cladding alloy and its effect on creep properties

R. C. ECOB, R. C. LOBB
CEGB Berkeley Nuclear Laboratories, Berkeley, Gloucestershire, GL13 9PB, UK
V. L. KOHLER*
Department of Metallurgy and Materials Science, University of Cambridge, CB2 3QZ, UK

The ageing of a 20/25 Nb stainless steel AGR fuel cladding alloy at 1023 or 1123 K is shown to produce small but significant changes in constant stress uniaxial creep behaviour in tests at 1023 K. The present paper is addressed to a correlation of the observed creep behaviour with the microstructural developments caused by the ageing treatments and the subsequent thermal exposure to 1023 K during creep testing. In the present alloy, NbC is unusually unstable with respect to G-phase ($Ni_{16}Nb_6Si_7$), with the latter forming more rapidly and at higher temperature than in other comparable materials in the absence of irradiation. Consideration is given to the reasons for this. It is shown that the G-phase particles, in contrast to those of NbC, are deformable at the 1023 K creep testing temperature. The creep behaviour is interpreted in terms of this observation, together with those of the progress of the NbC to G-phase transformation with ageing/creep, and the particle distributions thereby produced.

1. Introduction

Lobb [1] has recently investigated the relationship between the creep behaviour and heat treatment of a niobium stabilized 20 wt % Cr–25 wt % Ni stainless steel (termed 20/25 Nb) AGR fuel cladding alloy. The heat treatments to which the material was subjected, following a 3.6 ksec recrystallization anneal in hydrogen at 1203 K, were of 3.6 or 10.8 Msec at 1023 or 1123 K in argon, and formed a control series for a study of the effects on creep behaviour of oxidation in reactor coolant gas under the same thermal conditions. The argon controls showed small but significant alterations in creep behaviour as a function of ageing treatment when tested over a range of stresses at 1023 K.

The present work was undertaken with the object of correlating the microstructural developments which occur during ageing with the changes in creep properties for which they are responsible. It will be shown below that the dominant metallurgical feature of the steel examined in the temperature range used is the instability of NbC precipitates with respect to G-phase. The latter, a nickel–niobium silicide, is usually observed to form as an intragranular precipitate only either during irradiation or during protracted thermal exposures at lower temperatures (e.g. 713 to 973 K) (e.g. [2]), but because it *does* form in AGR fuel cladding materials under these circumstances, a knowledge of its effects on mechanical properties is of importance.

The present paper shows how Lobb's creep results can be interpreted in terms of those effects, and also gives consideration to the unusual prevalence of G-phase in the present steel at ageing temperatures of 1023 to 1203 K.

2. Summary of Lobb's results [1]

The alloy taken from an early cast of end-cap material of chemical composition (supplied with the alloy by British Nuclear Fuels Ltd) shown in Table I, was given one of five heat treatments prior to creep testing. All the specimens were recrystallized for 3.6 ksec in hydrogen at 1203 K, and one batch was tested in this condition. As above, four other batches were pre-aged for 3.6 or 10.8 Msec in argon at 1023 or 1123 K.

The results of constant-stress creep testing of the as-recrystallized and 3.6 Msec pre-aged materials at 1023 K over a range of stresses are shown as a plot of minimum creep rate against applied stress on log–log scales in Fig. 1. They can be summarized as follows.

Material aged for 3.6 ksec at 1203 K displays a stress component of the creep rate of ~ 4.3. Ageing in argon for 3.6 or 10.8 Msec at 1023 K causes increases in the creep rates over the whole stress range, with the stress exponent rising to ~ 4.7. Treatment for the same times at 1123 K leads to similar softening at high stress, but *decreases* in creep rate at low stress: the stress exponent is increased to ~ 5.6. None of the ageing treatments produces any deterioration in creep ductility as compared to the as-annealed material (3.6 ksec at 1203 K), with the strain at the onset of tertiary creep taking values of $\sim 40\%$ in all cases.

*Present address: CEGB, Berkeley Nuclear Laboratories, Berkeley, Gloucestershire GL13 9PB, UK.

0022–2461/87 $03.00 + .12

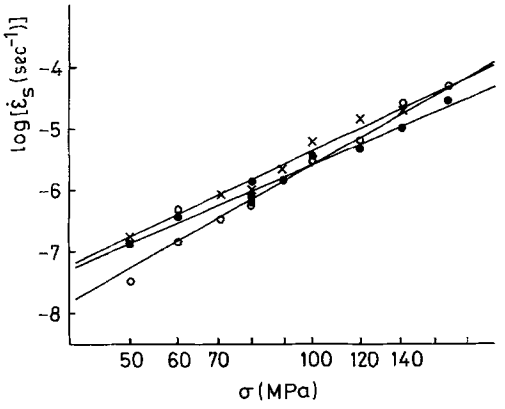

Figure 1 The creep data of Lobb [1], plotted as a minimum creep rate against applied stress on log–log scales. (●) 3.6 ksec, 1203 K; (x) 3.6 ksec, 1203 K + 3.6 Msec, 1023 K; (○) 3.6 ksec, 1203 K + 3.6 Msec, 1123 K.

3. Experimental procedure

Specimens from the above investigation were examined using a variety of techniques including transmission and scanning electron microscopy, optical microscopy, energy-dispersive X-ray analysis (EDS) and laser microprobe mass analysis (LAMMS) (see Section 4.3). The microstructures were also examined following a number of further heat treatments which are detailed where the results are discussed in the following section.

TABLE I Chemical composition of alloy (wt %)

Cr	Ni	C	Mn	Si	Nb	S	Ti	Fe
20.4	25.1	0.02	0.70	0.56	0.60	0.007	< 130 p.p.m.	bal

4. Results and discussion

4.1. Identification of G-phase

G-phases in general have formulae of the form $A_{16}B_6C_7$, where A and B are transition elements and C a Group IV element such as silicon or germanium: they have a face-centred cubic unit cell (structure type $D8_a$, space group Fm3m) containing 116 atoms (e.g. [3, 4]). Powell and co-workers [2, 5] have shown that in 20/25 Nb Component A is nickel, Component B is predominantly niobium with small contributions from iron and chromium, and Component C is silicon. The lattice parameter is ~ 1.12 nm.

In the present work, G-phase particles were readily and uniquely identifiable using a combination of microdiffraction and EDS analysis. Figs 2a and b show microdiffraction patterns from G-phase in ⟨0 0 1⟩ and ⟨1 1 1⟩ zone axis orientations, respectively. The former follows unambiguous differentiation between the Fm3m space group of G-phase and the Fd3m space group of M_6C (see figure caption). The significance of this arises because Powell [2] postulates that G-phase has often in the past been erroneously identified as M_6C, which would explain the infrequency of reports of its formation. Together, the two patterns of Fig. 2

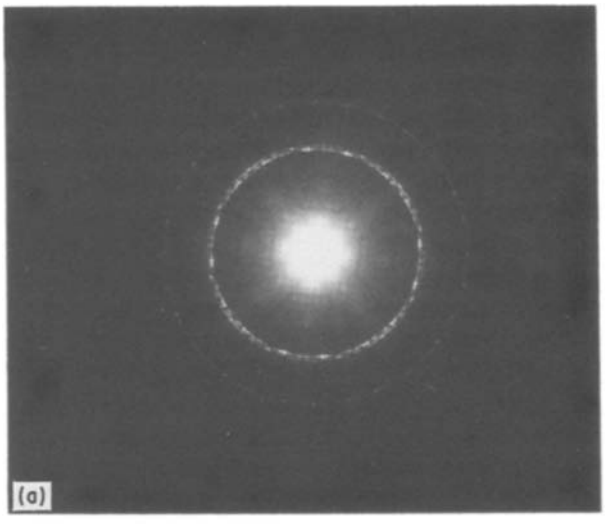

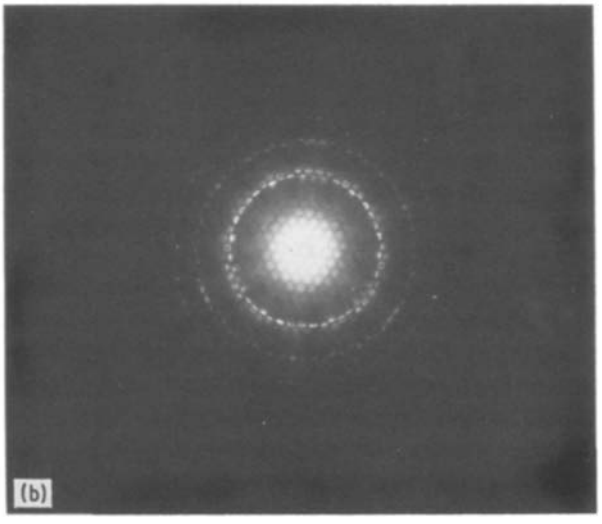

Figure 2 (a) ⟨0 0 1⟩ microdiffraction pattern from a G-phase particle; (b) ⟨1 1 1⟩ microdiffraction pattern from a G-phase particle; (c) typical EDS spectrum from a G-phase particle. The microdiffraction pattern of (a) displays the same square arrangement of reflections in the zero-order Laue layer (centre) and in the first-order Laue zone ring. This proves that the structure is not diamond cubic (space group Fd3m as for M_6C), for which the systematic absences in the two layers are different [6]. The angular spacing x of reflections $h\,k\,l$ in the zero layer is equal to twice the Bragg angle, $x = 2\sin^{-1}[\lambda(h^2 + k^2 + l^2)^{1/2}/2a]$ where λ is the electron wavelength and a the lattice parameter. The angular radius of the Nth Laue zone ring, r, is determined by the spacing of the reciprocal lattice layers parallel to the incoming electron beam direction $[u\,v\,w]$: $r = 2\sin^{-1}[N\lambda/2a(u^2 + v^2 + w^2)^{1/2}]^{1/2}$. Knowing λ(3.34 pm), $[u\,v\,w]$ and $h\,k\,l$ it is thus possible to calculate the lattice parameter. The patterns of (a) and (b) are consistent with a = 1.12 nm.

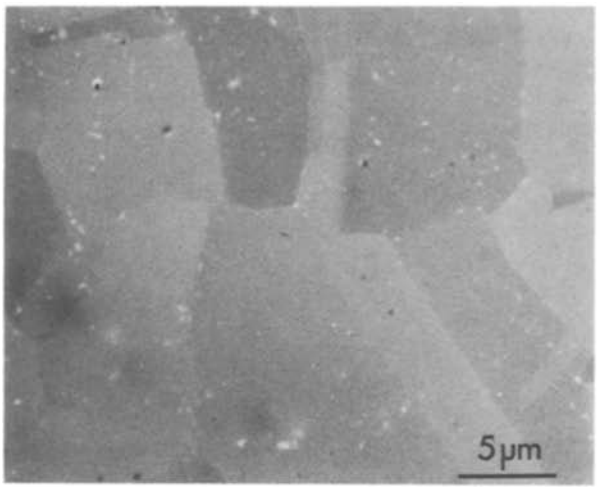

Figure 3 Backscattered electron (BSE) image obtained from a thin foil of material in the as-annealed condition (3.6 ksec at 1203 K).

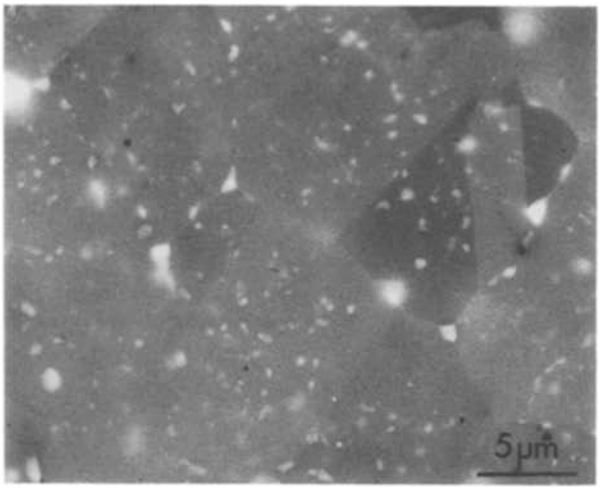

Figure 4 BSE image obtained from a thin foil of material pre-aged for 3.6 Msec at 1123 K.

allow calculation of the lattice parameter (again, see figure caption) as ~ 1.12 nm.

Fig. 2c shows a typical EDS spectrum from a G-phase particle, with peak heights from Ni(K), Nb(L) and Si(K) in the ratios $\sim 2:1:1$ (cf. Fig. 5 of [5]). This spectrum was obtained from a thin foil specimen, and so it is not certain whether the small iron and chromium peaks arise from the particle or from electron beam spreading into the surrounding matrix. Not withstanding this uncertainty, the important point in the present context is that G-phase particles can be identified with no ambiguity.

4.2. Microstructures produced by heat treatment

4.2.1. Heat treatment for 3.6 ksec, 1203 K only

The "as-received" initial condition of the material is after a recrystallization anneal of 3.6 ksec at 1203 K. Fig. 3 shows an overview of the microstructure, which consists of an equiaxed austenite grain structure with a dispersion of intragranular NbC and intergranular NbC and G-phase. TEM has shown that the NbC particles do not display an orientation relationship with the matrix, which suggests that the population is of "residual" NbC, i.e. precipitates which formed during manufacture of the as-supplied sheet where intermediate annealing temperatures are below the NbC solvus, and around which the matrix has finally recrystallized at 1203 K.

4.2.2. Recrystallization anneal plus pre-ageing at 1123 K

Fig. 4 shows the microstructure produced by the pre-ageing treatment of 3.6 Msec at 1123 K. Here all the particles are of G-phase and display EDS spectra as shown in Fig. 2c above. The implication is that at 1123 K G-phase is the equilibrium precipitate in the present alloy: no other type of particle has been observed. This is in marked contrast to the behaviour discussed by Powell [2], where $M_{23}C_6$ was frequently observed to form in association with G-phase as a result of the rejection from the latter of chromium and carbon. Further consideration of this point is given in Section 4.3 below. The G-phase particles display no reproducible orientation relationship with the austenite, and the particle–matrix interfaces are thus incoherent.

It is apparent from a comparison of Figs 3 and 4 that the development of a second-phase population composed entirely of G-phase has produced a considerable increase in the particle volume fraction with respect to the as-recrystallized material. An estimate of this increase, associated with the transformation from NbC to G-phase, can be obtained as follows.

The volume of second phase per niobium atom is given by a^3/n, where a is the relevant lattice parameter and n the number of niobium atoms per unit cell (respectively 0.447 nm and 4 for NbC, 1.12 nm and 24 for G-phase). If the total potential number of niobium atoms contained in each phase is then taken to be equal to the atomic fraction of carbon for NbC and of niobium for G-phase, the ratio of volume fractions is given by

$$\frac{f_G}{f_{NbC}} = \frac{a_G^3}{24}\left(\frac{\text{wt \% Nb}}{W_{Nb}}\right)\Big/\frac{a_{NbC}^3}{4}\left(\frac{\text{wt \% C}}{W_C}\right)$$

where W is the atomic weight. The ratio (wt % Nb)/(wt % C) (the stabilization ratio) in the present material is ~ 30 (see Table I), yielding a volume fraction ratio of $\sim 10:1$.

4.2.3. Recrystallization anneal plus pre-ageing at 1023 K

No specimens which had been given only a pre-ageing treatment at 1023 K following the recrystallization anneal were available, since all had been creep tested. The testing temperature was also 1023 K, however, and so the microstructural changes during creep correspond simply to a continuation of those produced during pre-ageing. The latter can therefore be inferred (see Section 4.4) as again consisting of the development of a particle population composed entirely of G-phase, with the exception of a few large intergranular precipitates of σ-phase.

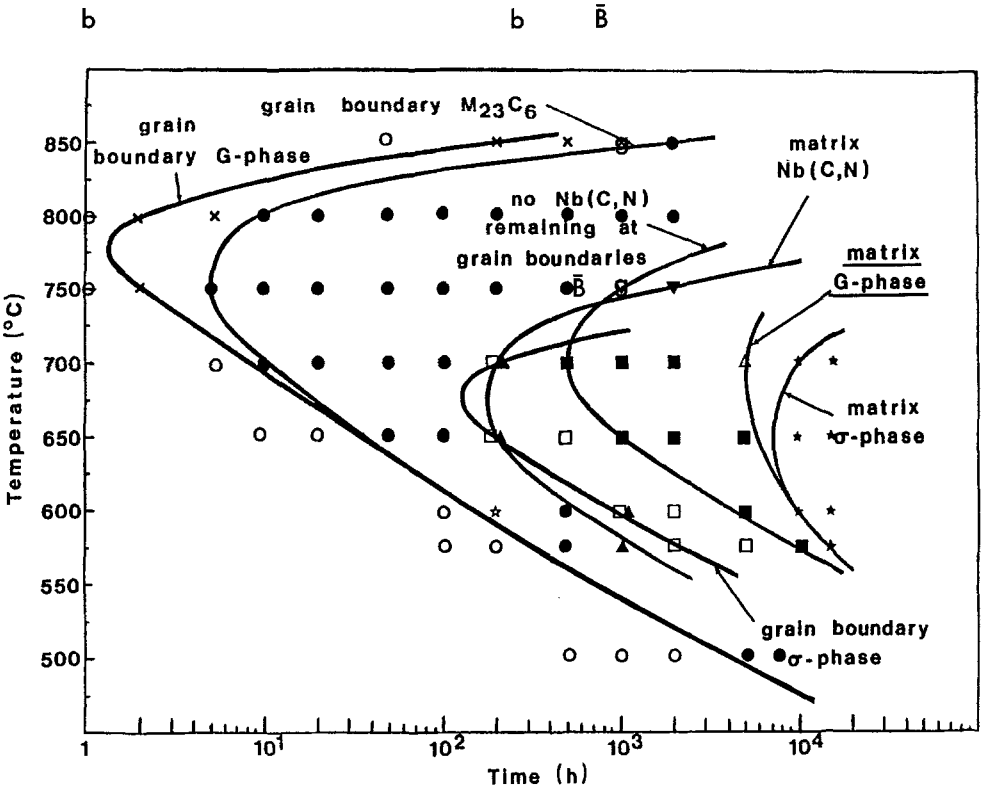

Figure 5 Time–temperature–precipitation diagram for the alloy studied by Powell and co-workers, reproduced from [5]. Superimposed are the results of treatment of the present alloy, where (b) and (g) denote the occurrence of grain-boundary and intragranular G-phase, respectively. ($\bar{B}$) refers to the absence even of grain-boundary G-phase in the Ecob and Gilmour alloy [7]. The tendency for G-phase formation therefore decreases in the sequence present alloy–Powell alloy–Ecob and Gilmour alloy. (○) Residual Nb(C, N), (☆) + g.b. $M_{23}C_6$. (×) Residual Nb(C, N) + g.b. G-phase, (●) + g.b. $M_{23}C_6$, (▲) + matrix Nb(C, N), (□) + g.b. σ-phase. (■) G-phase + $M_{23}C_6$ + matrix Nb(C, N) + σ-phase, (△) + matrix G-phase, (★) + matrix σ-phase. (▽) g.b. G-phase + g.b. $M_{23}C_6$, (▼) + matrix Nb(C, N).

4.3. Occurrence of G-phase–comparison with other 20/25 Nb alloys

It has already been intimated that the occurrence of G-phase is more prevalent in the present material than in other, nominally comparable, 20/25 Nb alloys. Powell and co-workers [2, 5] have reviewed previous reports of the phase, which, as mentioned earlier, are rare. From their own work, they construct a time–temperature–precipitation diagram showing the times at temperature in which the various precipitate populations are established (Fig. 5). They observe standard C-curve behaviour, where longer times are required for a given transformation at higher temperatures (due to low driving forces) and at lower temperatures (due to slow diffusion rates) than at the "nose" where the transformation rate is maximized. They identify the "noses" for G-phase formation as occurring at ~3.6 ksec, 1048 K and ~18 Msec, 973 K for grain-boundary and matrix precipitation, respectively. At the highest temperature they investigated (1123 K), only grain-boundary G-phase was formed; extrapolation of the appropriate C-curve would suggest an upper temperature limit for intergranular G-phase between 1123 and 1173 K.

From the foregoing it is apparent that the present alloy behaves significantly differently to that studied by Powell, with intergranular G-phase observed after 3.6 ksec at 1203 K and matrix precipitates after 3.6 Msec at both 1123 and 1023 K, with no residual NbC remaining after the latter treatment. In other words, the NbC in the present case appears to be considerably more unstable with respect to G-phase, with the latter forming more rapidly and at higher temperatures. It should be noted that the upper temperature limit for matrix G-phase formation in the present alloy appears to be between 1123 and 1203 K: heat treatment at 1203 K for 1.01 Msec produces coarsening of the matrix NbC, but no evidence of G-phase formation except at grain boundaries.

Recently Ecob and Gilmour [7] have studied the behaviour of a third 20/25 Nb cladding alloy which displays no G-phase formation after treatment at 1203 K for times up to 2.69 Msec or at 1023 K for ~2 Msec. The indications are thus that this material is even more resistant to G-phase formation than that investigated by Powell and co-workers [2, 5] (Fig. 5).

These three alloys have been subjected to a LAMMS analysis. This technique involves the generation of a frequency spectrum of ion masses from a time-of-flight mass spectrometer, using a laser pulse to produce the ion population from the polished specimen surface. The spatial resolution of the technique in the surface plane is ~5 μm, which is large enough for the elemental analyses to be regarded as characteristic of the bulk material.

Typical spectra from the present alloy and from that investigated by Ecob and Gilmour [7] (after ageing 7.2 ksec in hydrogen at 1203 K in both cases) are given in Fig. 6, and the results of the comparative analyses are given in Table II. It should be noted that these are not quantitative alloy compositions, but that the ratios of the peak areas can be directly compared.

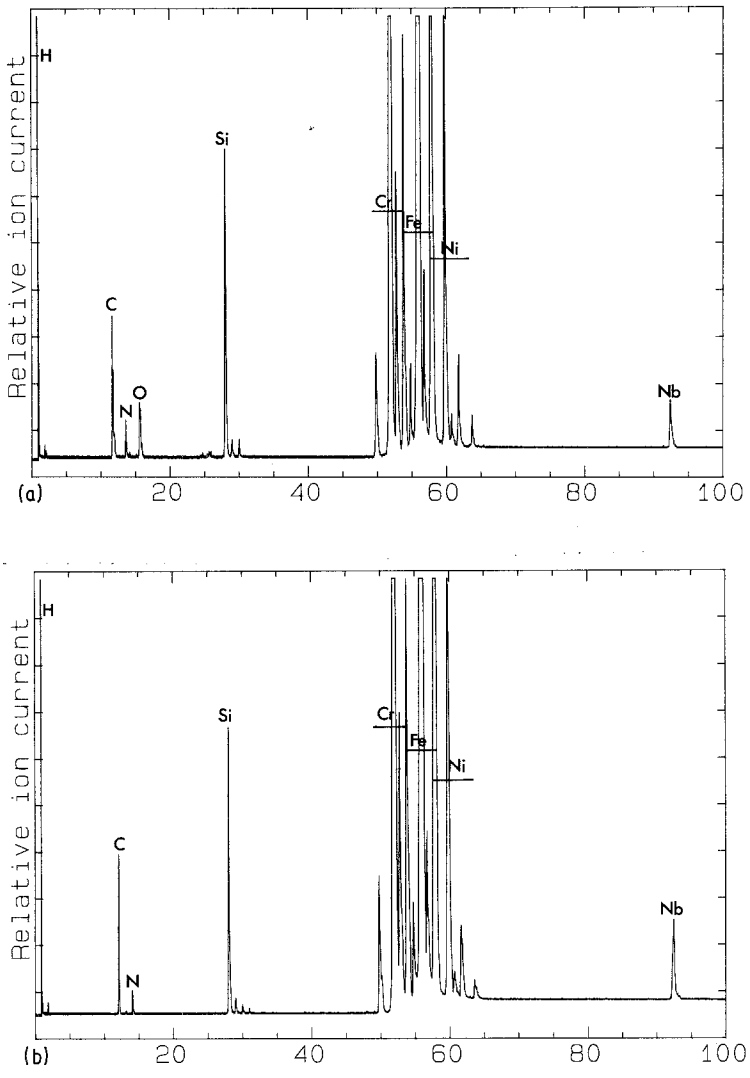

Figure 6 Typical LAMMS spectra obtained from (a) the present alloy; (b) the Ecob and Gilmour alloy, heat-treated 7.2 ksec at 1203 K in hydrogen. The horizontal axis is ion mass per ion charge; all the labelled peaks are for singly charged ions.

It can be seen that there is no significant difference between the levels of nickel or silicon, normalized with respect to chromium; the ratios of niobium to carbon are likewise comparable, although the scatter on these data is rather large because it is not possible to adjust the incoming laser power for optimal detection efficiency of both these elements at once.

The only significant reproducible difference in the spectra from the two materials is in the level of oxygen, which is very much higher in the present alloy (Table II and Fig. 6). The tentative conclusion, which clearly requires further work to be substantiated and quantified, is that an increased oxygen content leads to a greater instability of NbC with respect to G-phase. Analysis of the Powell alloy, intermediate in behaviour with respect to G-phase formation, yields an intermediate oxygen content (O/Cr = 0.14 ± 0.04), supporting the present postulate.

TABLE II Results of LAMMS analyses (ratios of peak areas)

Elements	Ratio of peak areas	
	Present alloy	Ecob and Gilmour alloy
Ni/Cr	0.33 ± 0.03	0.34 ± 0.05
Nb/Cr	0.12 ± 0.06	0.10 ± 0.05
Nb/C	0.41 ± 0.68	0.35 ± 0.28
Si/Cr	4.37 ± 2.6	4.33 ± 2.3
O/Cr	0.52 ± 0.05	0.03 ± 0.004

It is not immediately clear why oxygen should destabilize NbC, but some indication can be obtained from Fig. 7, which shows EDS spectra from NbC particles in the present and the Ecob and Gilmour alloys after ageing for 7.2 ksec at 1203 K. The spectrum from the latter material shows Nb(L) and Nb(K) peaks, with small contributions from matrix chromium, iron and nickel. These matrix peaks are much larger in the spectrum from the present alloy because the particle analysed was smaller: the two spectra have been arranged so that the niobium peaks are of the same height in each.

The significant difference between these spectra is the presence of an Si(K) peak in Fig. 7a from the present alloy which is absent in Fig. 7c from the Ecob and Gilmour material where NbC is more stable. While it is clearly reasonable to suppose that an enhanced silicon level in or around NbC particles will tend to drive the transformation to G-phase, it should be noted again that the bulk silicon contents of the two alloys are not significantly different. The implication is that the segregation of silicon is encouraged by the presence of oxygen, which in turn may suggest that oxygen itself is segregating to the NbC particles.

The explanation may in reality be more complex, since if silicon follows oxygen in segregating to NbC the most favourable reaction would be expected to involve the chemical combination of the two.

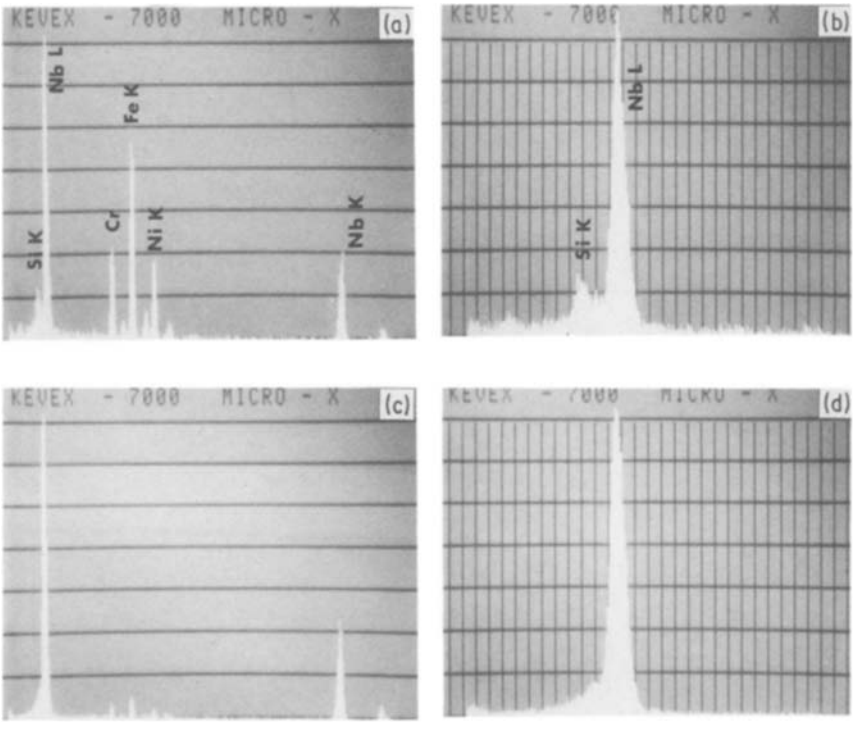

Figure 7 Typical EDS spectra obtained from NbC particles in specimens-heat treated for 7.2 ksec at 1203 K (a, b) the present alloy; (c, d) the Ecob and Gilmour alloy. The enhanced silicon peak from the present alloy is seen more clearly on the expanded scale of (b).

Nevertheless, the present work has shown that an increased silicon concentration in or near NbC *is* associated with its instability, and has implied that an increased bulk oxygen content may be the cause. Note that the role of silicon segregation in assisting G-phase formation is consistent with its increased prevalence after irradiation (e.g. [2]).

Fig. 8 shows a set of four EDS spectra obtained from particles in a single specimen of the present alloy which had been given a recrystallization anneal and exposed to 1023 K during a creep test at 90 MPa. All of the particles have the G-phase structure (as confirmed by microdiffraction) but cover a wide range of composition. This implies first that the NbC to G transformation occurs *in situ* (as observed by Powell *et al.* [5]) which would further support the idea that the apparent stability of NbC is determined by the extent of segregation. Further, the very high levels of Nb in "recently transformed" G-phase particles (uppermost spectrum in Fig. 8) indicate that small compositional changes are sufficient to allow the transformation. This suggests that carbon may be soluble in G-phase, which would explain the absence of any carbide particles after ageing at 1023 or 1123 K. Further, if there is taken to be a critical level of silicon needed to drive the structural transformation, it is also possible to interpret the microstructure observed in the present alloy after heat treatment at 1203 K, where G-phase is only formed at grain boundaries. This arises because the critical level can only be achieved at this temperature by particles using boundaries as "collector plates" for silicon segregation, i.e. by increasing the local concentrations of silicon as the latter segregates to the boundary, rather than directly to the particle. That the *matrix* NbC shows no signs of transformation to G-phase even after 1.01 Msec at 1203 K suggests that the difference in behaviour at grain boundaries and in the matrix is not due simply to different kinetics, so that an explanation based on enhanced silicon segregation is again in accord with experimental observation.

In summary, it can be concluded that the unusual prevalence of G-phase in the present material as compared to other 20/25 Nb alloys arises because the segregation of silicon to NbC particles, clearly a prerequisite for G-phase formation, occurs under a higher driving force, i.e. faster and at higher temperature. Such an increased driving force could result from an increased bulk silicon content, but the two alloys investigated here are comparable in this respect. Indeed the only difference between them appears to be in their oxygen contents, and it has therefore been tentatively suggested that therein lies the cause of their very different behaviours.

4.4. Changes in microstructure during creep testing at 1023 K

The microstructural changes observed during creep testing at 1023 K depend on the applied stress because of its influence on the duration of the test. For that reason, a set of specimens was examined which had been exposed to 1023 K during tests at 50, 100 and 140 MPa for times of order 10^6, 10^5 and 10^4 sec, respectively, following each of the three treatments 3.6 ksec at 1203 K, 3.6 Msec at 1123 K and 3.6 Msec at 1023 K. The phases observed are summarized in Table III.

4.4.1. Specimens treated at 1203 K

Specimens subjected only to the initial recrystallization anneal of 3.6 ksec at 1203 K transform with increasing creep exposure time at 1023 K from the low volume fraction matrix NbC–grain-boundary G-phase microstructure (Section 4.2.1) towards the G-phase–σ-phase condition characteristic of the 1023 K pre-aged material (Fig. 9). Indeed the transformations

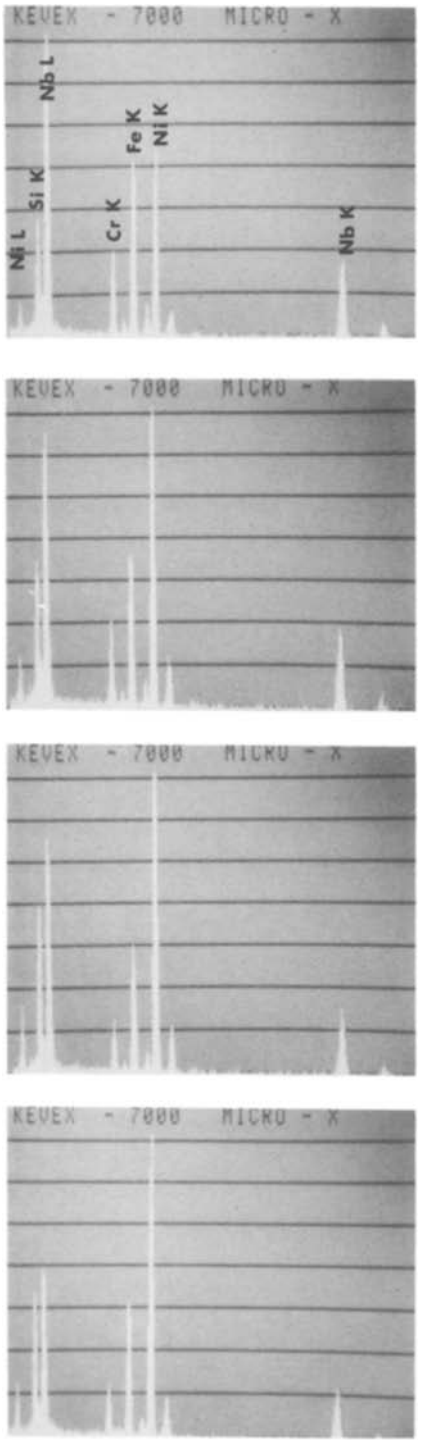

Figure 8 Four EDS spectra obtained from G-phase particles in an as-annealed specimen exposed to 1023 K during a creep test at 90 MPa. The Ni : Nb : Si peak height ratios vary from ~2 : 1 : 1 (cf. Fig. 2c) to ~1 : 2 : 1.

observed during creep at 1023 K here must be the same as those which occur during the earlier stages of the pre-ageing treatments.

Following the recrystallization anneal at 1203 K, the kinetics of the transformation from NbC to G-phase at 1023 K appear to be slow enough that some residual NbC remains after 100 ksec (100 MPa), though the transformation is complete after 1 Msec (50 MPa). In the latter case, however, the specimens contain a population of fine reprecipitated NbC, which is distinguishable from residual NbC by virtue of its cube–cube orientation relationship with the matrix. Presumably this population develops in response to a renewed supersaturation with respect to NbC on temperature reduction from 1203 to 1023 K.

4.4.2. Specimens pre-aged at 1023 K for 3.6 Msec

Thermal exposure during the creep tests here represents simply a continuation of the pre-ageing treatment, and so the major effect is an overall coarsening of the microstructure (Fig. 10). The reprecipitation of NbC discussed above is completed during the pre-ageing, and the intergranular particles observed here are exclusively G-phase, even after the shortest total exposure to 1023 K of 3.6 Msec ageing plus ~10 ksec creep.

The implication of the latter observation is that the reprecipitated NbC particles transform to G-phase, which in turn suggests that the equilibrium volume fraction of G-phase can only be established following the development of the metastable NbC population. Accordingly, the volume fraction of G-phase appears to increase in the time interval ~1 Msec (Fig. 9c) to ~3.61 Msec (Fig. 10a) at 1023 K. It can be inferred that G-phase cannot nucleate directly but only on pre-existing NbC, i.e. the transformation always occurs *in situ*. The differences in the distribution of G-phase particles produced by the various heat treatment routes used in the present work must therefore be attributed to the way in which the prior NbC populations, both residual and reprecipitated, develop with time at each temperature.

There is also a microstructural correlation between G-phase and σ-phase. The latter is only observed at grain boundaries, and the particles formed during pre-ageing tend to coarsen during creep. Fig. 11 shows one such particle apparently growing around smaller G-phase precipitates. This is entirely in accord with expectation in that the segregation of nickel to G-phase enriches the surrounding matrix in iron and chromium, thus encouraging the nucleation of σ-phase.

4.4.3. Specimens pre-aged at 1123 K for 3.6 Msec

Exposure to 1023 K during testing here leads to an increase in volume fraction of G-phase towards the equilibrium value at the lower temperature (Fig. 12). This increase tends to occur by growth and coarsening of the particles formed at 1123 K, however, rather than by the nucleation of more particles, which in the light of the discussion given in Section 4.4.1 above suggests that no reprecipitation of NbC occurs, and indeed none has been observed. Hence although the volume fractions of G-phase in both the 1023 and 1123 K pre-aged specimens would be expected to be identical given long enough exposure to 1023 K during the creep test, the particle distributions are different. Comparison of Figs 13a and b shows clearly that after creep tests at 50 MPa there are fewer, larger G-phase precipitates in the specimen aged at higher temperature.

Some grain-boundary σ-phase is again formed; the particles are smaller here than in the 1023 K pre-aged specimens because no σ-phase is formed during

TABLE III Summary of phases observed following heat treatments and creep testing

Heat treatment route			Precipitates*					
Anneal	Pre-age	Creep at 1023 K	g.b. NbC	Matrix NbC		g.b. G	Matrix G	g.b. σ
				Residual	Reprecipitated			
3.6 ksec, 1203 K			√	√	×	√	×	×
		+ 140 MPa, 10^4 sec	√	√	×	√	√	×
		+ 100 MPa, 10^5 sec	√	√	×	√	√	√
		+ 50 MPa, 10^6 sec	√	×	√	√	√	√
	+ 3.6 Msec, 1123 K		×	×	×	√	√	×
		+ 140 MPa, 10^4 sec	×	×	×	√	√	×
		+ 100 MPa, 10^5 sec	×	×	×	√	√	√
		+ 50 MPa, 10^6 sec	×	×	×	√	√	√
	+ 3.6 Msec, 1023 K		×	×	×	√	√	√
		+ 140 MPa, 10^5 sec	×	×	×	√	√	√
		+ 50 MPa, 10^6 sec	×	×	×	√	√	√

*g.b. = grain boundary.

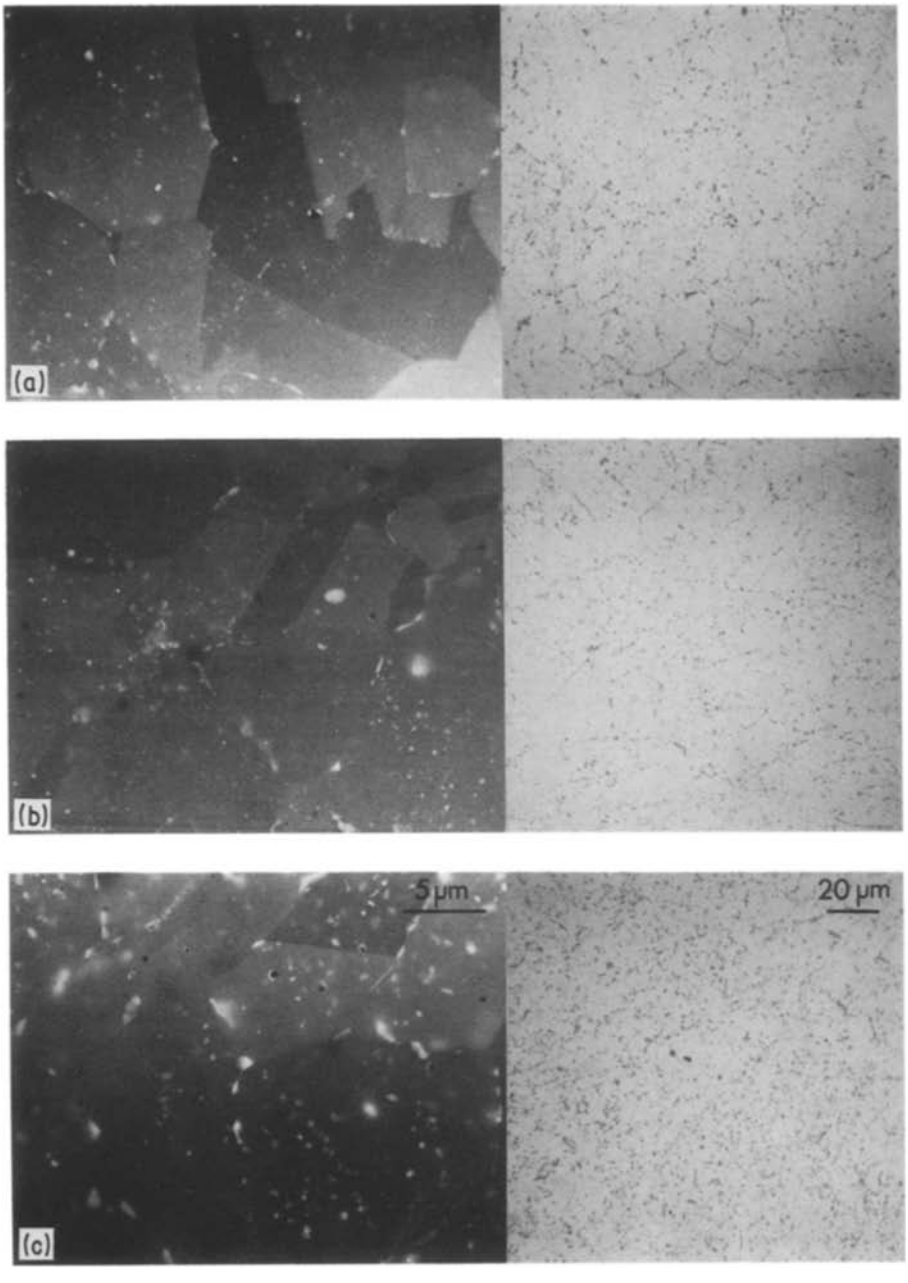

Figure 9 BSE (left) and optical microscope (right) images of as-annealed (3.6 ksec, 1203 K) material after exposure to 1023 K during creep tests at (a) 140 MPa, (b) 100 MPa, (c) 50 MPa.

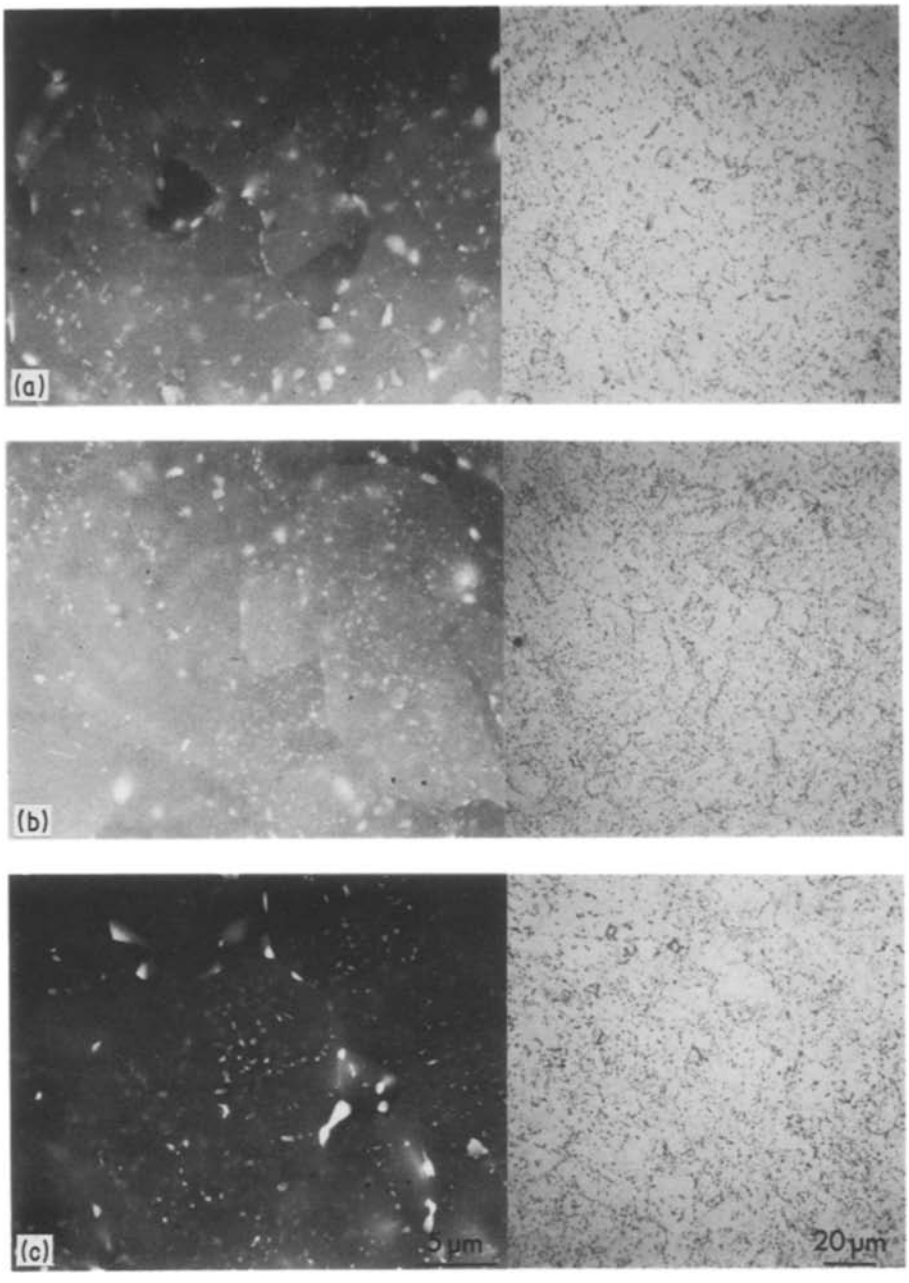

Figure 10 BSE (left) and optical microscope (right) images of material pre-aged for 3.6 Msec at 1023 K, and further exposed to 1023 K during creep tests at (a) 140 MPa, (b) 100 MPa, (c) 50 MPa.

pre-ageing at 1123 K and the exposure to the lower temperature is shorter.

4.5. Effects of G-Phase formation on creep properties

4.5.1. Creep rate

It has already been pointed out that the G-phase formed during pre-ageing at 1023 and 1123 K has a volume fraction of order ten times higher than that of the NbC it replaces. In the creep tests at high stress, however, the pre-aged material displays significantly higher minimum creep rates, e.g. by a factor of ~ 2 at 140 MPa (Fig. 1). It can immediately be concluded that G-phase provides very much less strengthening (creep resistance) per volume fraction than NbC.

At low stress (e.g. 50 MPa), the creep properties of the material treated for 3.6 ksec at 1203 K and 3.6 Msec at 1023 K tend to become comparable (Fig. 1). This can be rationalized in terms of the observation that the microstructures likewise become

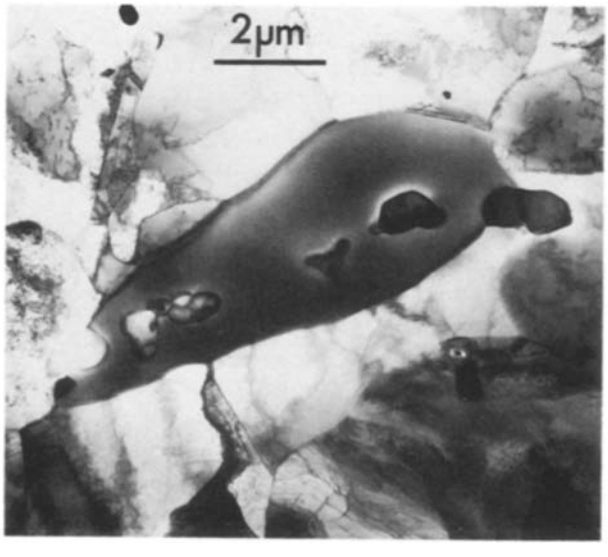

Figure 11 Bright-field transmission electron micrograph showing a large intergranular σ-phase particle enveloping smaller G-phase particles in a specimen pre-aged at 1023 K and crept at 100 MPa.

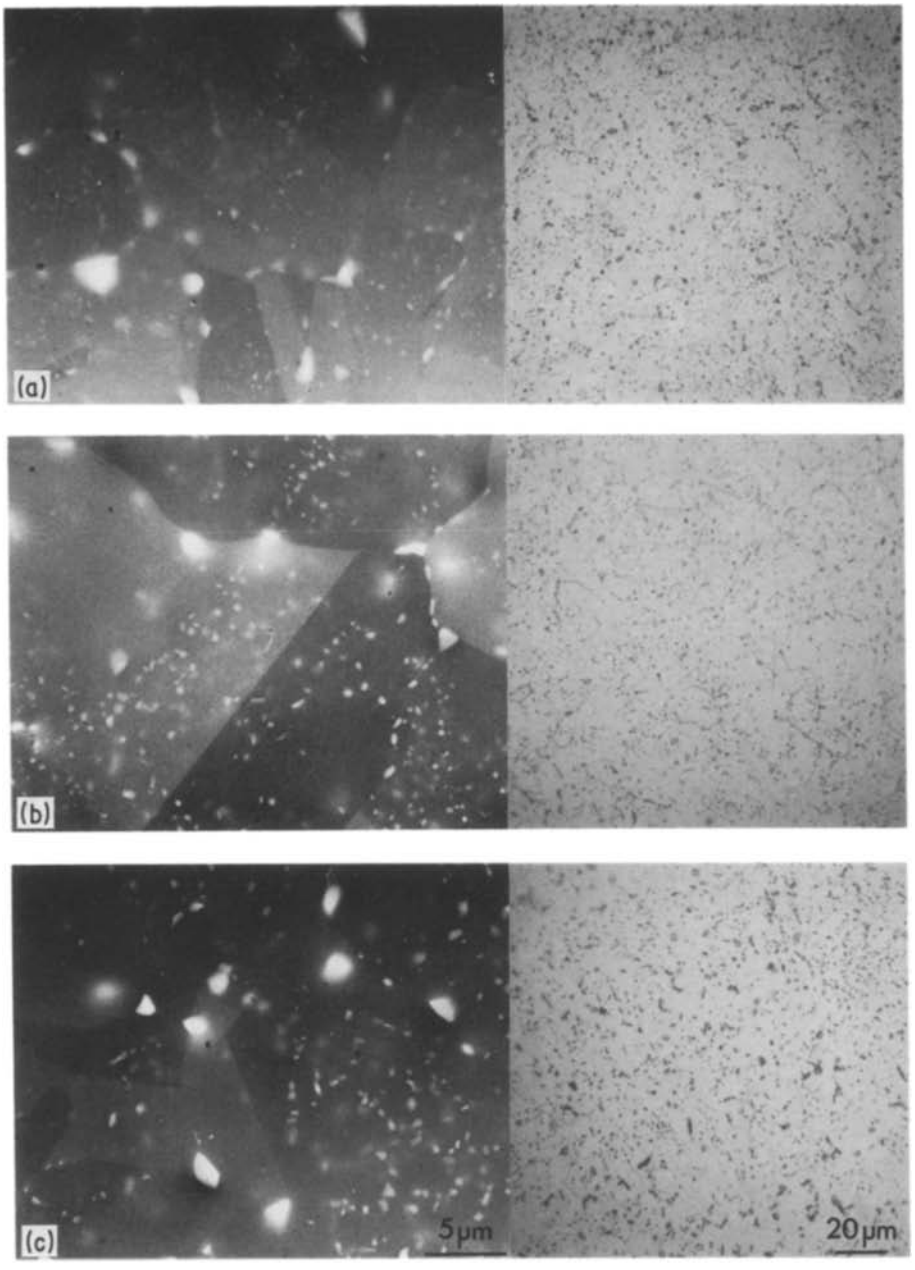

Figure 12 BSE (left) and optical microscope (right) images of material pre-aged for 3.6 Msec at 1123 K (cf. Fig. 4) and exposed to 1023 K during creep tests at (a) 140 MPa, (b) 100 MPa, (c) 50 MPa.

similar. As discussed above, the same microstructural developments occur in the as-recrystallized material during creep testing as in the pre-aged material prior to testing, and the total 1023 K exposure times of the two converge as the stress is decreased. The strengthening effect of the NbC which still exists after 3.6 ksec at 1203 K is thus lost during creep testing at 1023 K, with this softening occurring to a larger extent at low stress. The reprecipitation of NbC at times between $\sim$ 100 ksec and 1 Msec during creep testing may replace some of this strength, which explains the difference in minimum creep rate at 50 MPa. The principal effect of this reprecipitation, however, would be expected to be on the *shape* of the creep curve; further discussion of this is deferred to another report [7].

The creep data also demonstrate that at low stress the material pre-aged at 1123 K is stronger (i.e. has a lower minimum creep rate) than either the as-recrystallized or 1023 K pre-aged materials. As discussed earlier, the major microstructural difference after creep testing at 50 MPa is the coarser distribution of G-phase particles produced by the higher temperature pre-ageing treatment. If it is assumed that the volume fractions approach a constant value characteristic of equilibrium at 1023 K during the creep test, then it can be concluded that the strengthening effect of G-phase particles increases as their size and spacing increase. The implication is that unlike NbC they do not act as strong obstacles to dislocation motion, where decreased interparticle spacings lead to enhanced creep resistance, but rather that they are deformable (e.g. [8]).

Fig. 14 shows an intergranular G-phase particle in material pre-aged for 3.6 Msec at 1123 K and crept at 140 MPa. It can be seen that there are faults within it, one of which is bounded by a dislocation (which must therefore be a partial dislocation of the G-phase structure). Fig. 14 thus provides confirmation of the deformability of G-phase. It should be noted, however, that since no reproducible orientation relationship is

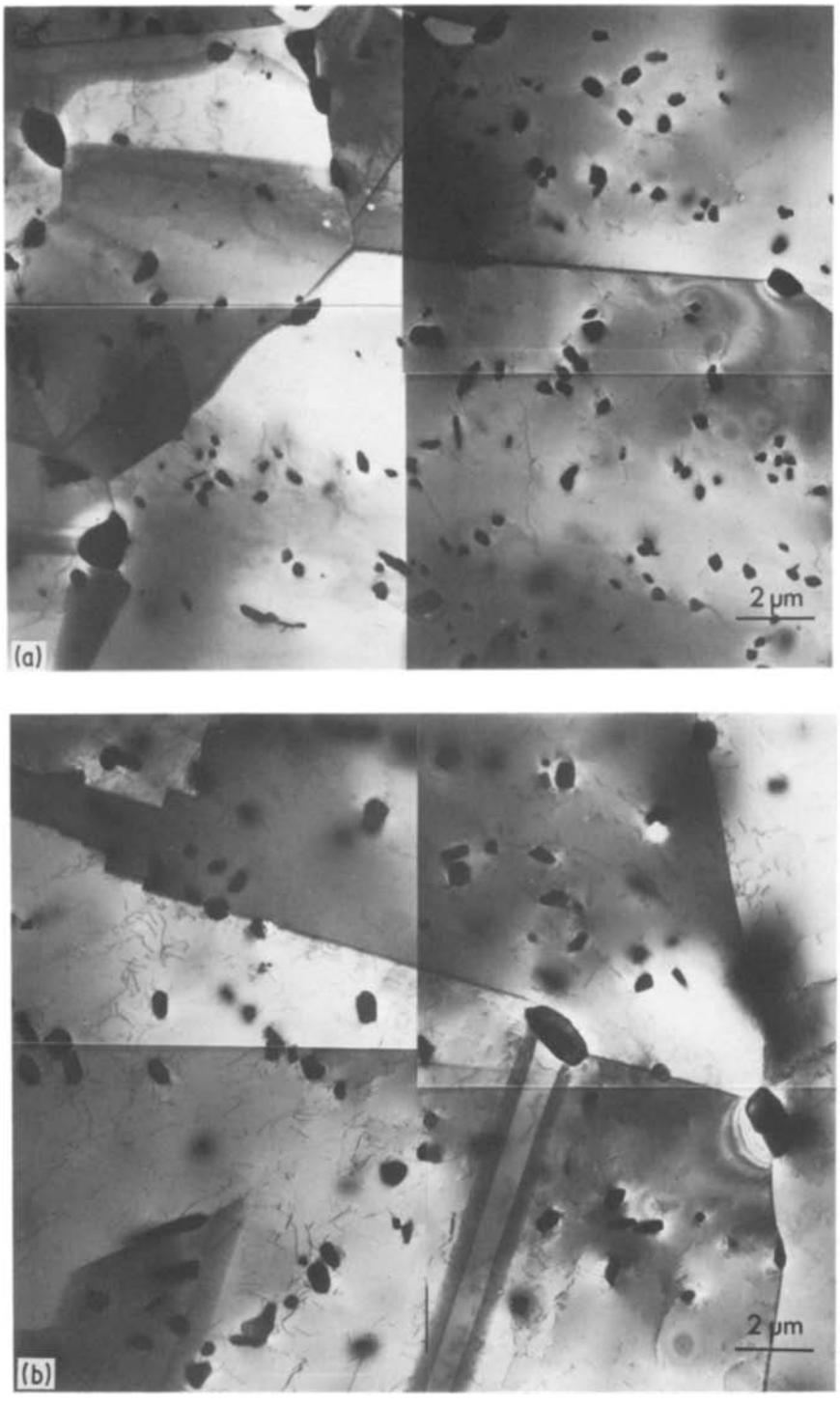

Figure 13 Bright-field transmission electron micrographs corresponding to the BSE images of Figs 10c and 12c, showing matrix G-phase distributions produced by exposure to 1023 K during creep tests at 50 MPa in material pre-aged at (a) 1023 K, (b) 1123 K.

observed between matrix and G-phase, the particles cannot be classically cut: matrix dislocations are geometrically unable to shear the particle simply by passing through them on essentially continuous slip planes. Nevertheless, it is apparent from Fig. 14 that dislocation activity within the particle is correlated with that in the matrix; the fault already discussed intersects the particle–matrix interface where a matrix dislocation array impinges upon it.

The yield stress of alloys containing deformable particles is usually taken to depend on r/l (e.g. [8]), where r is the radius of the particles and l their spacing. These two parameters are related via the volume fraction, which is also proportional to r/l. In the present case, therefore, the 1123 and 1023 K pre-aged materials would be expected to have approximately equal flow stresses in long-duration creep tests at 1023 K because the volume fractions of G-phase are likewise similar. It is therefore suggested that the difference in creep rates cannot be explained in terms of a difference in 'threshold (yield) stress" for particle deformation.

Fig. 15 shows a plot of applied stress against the reciprocal of the subgrain size measured in crept specimens of the two pre-aged materials, and indicates that the subgrain size, and by extension the matrix dislocation processes which lead to subgrain formation, are independent of the G-phase particle distributions, in contrast to the case of alloys containing undeformable particles (e.g. [9]). Further, it indicates

Figure 14 Bright-field transmission electron micrograph showing a G-phase particle containing a high density of faults. One fault (arrowed) is bounded by a dislocation, and intersects the particle–matrix interface where a matrix dislocation array impinges upon it.

that no change in mechanism, involving for example the deformation of small particles but not of large ones, can be invoked to explain the slower creep rates in the 1123 K pre-aged material.

The present suggestion is therefore that the reason for the difference in creep rates must be based only on the kinetics of the processes which allow matrix dislocations to overcome the obstacles represented by G-phase particles. That the latter are deformable means that a matrix dislocation gliding on a slip plane which intersects a particle will always be able to reach the incoherent particle–matrix interface (e.g. Fig. 14). As above, it will probably not be able to pass into the particle (although its arrival may lead to the nucleation of further dislocations within the G-phase), so that the matrix dislocation becomes pinned in that interface. It is possible that the particle-size dependence of the creep rate then arises because the movement through, and release from, the interface of the matrix dislocation is likely to require some diffusional rearrangement within the interface, the extent of which will increase as the particle size increases.

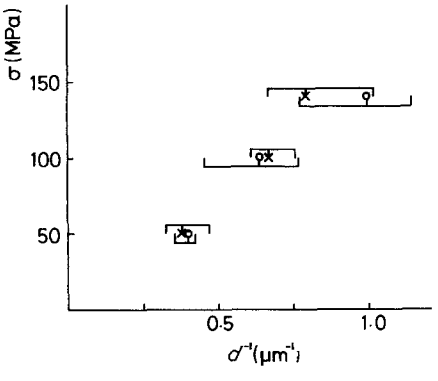

Figure 15 Applied stress plotted against the reciprocal of subgrain size, measured using transmission electron microscopy, for material pre-aged at (x) 1023 and (○) 1123 K for 3.6 Msec, in addition to 3.6 ksec at 1203 K.

Whatever the details of the dislocation mechanism which determine the particle-size dependence of the creep rate once G-phase is present, however, it is clear from the present work that the transformation from NbC to G-phase tends to lead to an increase in the creep rates at a given stress as strong obstacles are replaced by weak ones. That this is concluded from creep tests at 1023 K should *not* be taken to imply that G-phase particles will behave as weak obstacles at lower temperature. Yaney *et al.* [10], for example, concluded that Al_3Fe particles were deformed during creep of a rapidly solidified Al–Fe–Ce alloy at high temperatures in the range 523 to 823 K, and here the material was much weaker than oxide dispersion strengthened (ODS) aluminium in which the oxide particles are strong obstacles. At lower temperature, by contrast, the Al_3Fe particles were also undeformable, and their larger volume fraction meant that then the ODS aluminium was the weaker material. Exactly parallel behaviour might be expected in the present alloy, though clearly it would be necessary to perform lower temperature creep tests to prove it.

4.5.2. Creep ductility

As mentioned above, none of the heat treatments used in the present work produced any significant deterioration in creep ductility. Powell [2] similarly reports that the formation of G-phase, even in the form of very large particles elongated along grain boundaries, has no deleterious effect on strains to failure. While it might be expected that such microstructures would lead to early creep rupture, again the deformability of G-phase means that the compatibility stresses at grain boundaries can be relaxed more readily than in the presence of hard particles. In the present alloy, the grain-boundary G-phase particles do not grow as large as those produced by Powell (in longer times at lower temperatures), so that their effects on ductility are negligible. Once more this conclusion may not hold at lower temperature if the G-phase becomes effectively undeformable.

One respect in which the formation of G-phase may even be beneficial to creep ductility is in the suppression of secondary recrystallization resulting from the approximately tenfold increase in second-phase volume fraction and hence stronger pinning of grain boundaries. In their study, Ecob and Gilmour [7] observed the onset of secondary recrystallization after ~ 180 ksec heat treatment at 1203 K, and an almost completely secondarily recrystallized microstructure after ~ 2.7 Msec at the same temperature. The present alloy is very much more resistant to this abnormal grain growth at 1203 K (Fig. 16), but this may be due as much to the finer distribution of residual NbC as to the formation of grain-boundary G-phase at this temperature (Fig. 17). There is no evidence of secondary recrystallization after ageing of the present alloy for

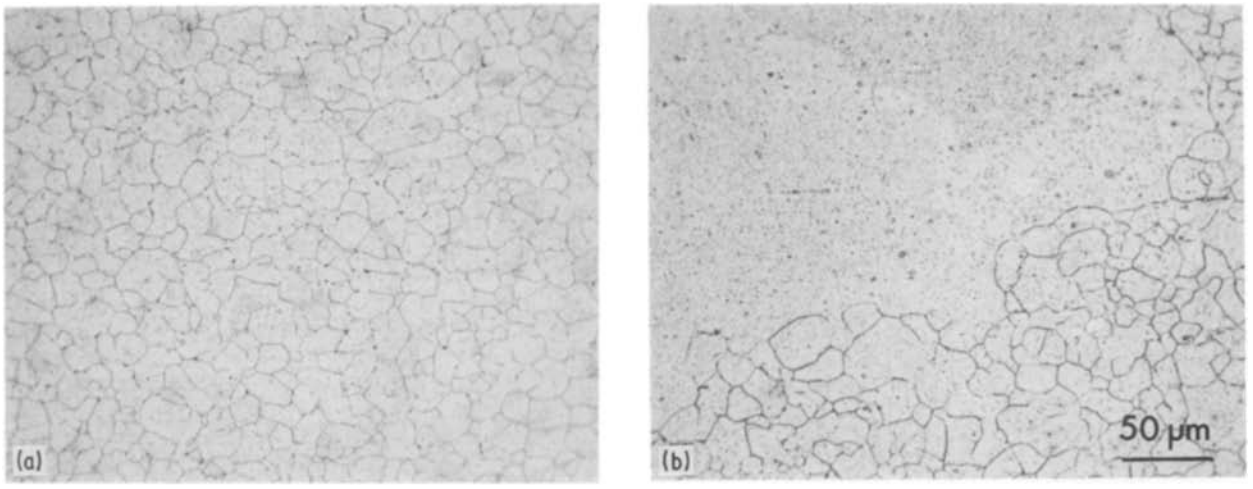

Figure 16 Optical microscopy images showing the grain structure of (a) the present alloy, (b) the Ecob and Gilmour alloy, after ageing for 1.01 Msec at 1203 K, and indicating the greater resistance of the former to secondary recrystallization.

10.8 Msec at 1123 K, where all the particles are of G-phase, but there are currently no comparable data on material in which NbC is stable.

5. Conclusions

Lobb [1] has reported constant-stress uniaxial creep data obtained by testing at 1023 K specimens of a 20/25 Nb AGR fuel cladding alloy in both as-annealed (3.6 ksec at 1203 K in hydrogen) and pre-aged (3.6 or 10.8 Msec at 1023 or 1123 K in argon) conditions. In the present work, the microstructures produced by these heat treatments and by subsequent thermal exposure to 1023 K during creep testing are examined. The following conclusions are reached:

1. In the present alloy, NbC is unusually unstable with respect to G-phase ($Ni_{16}Nb_6Si_7$), with the latter forming more rapidly and at higher temperature than reported in other comparable materials. G-phase precipitates occur at grain boundaries during treatment at 1203 K and throughout the microstructure at 1023 and 1123 K. Observations are presented which indicate that it can *only* form by transformation of pre-existing NbC particles. The instability of the NbC appears to be associated with the segregation thereto of silicon, but on the basis of laser microprobe mass analysis of the present alloy and another in which NbC is more stable, it is tentatively suggested that this may actually involve the co-segregation of silicon and oxygen.

2. It is shown that particles of G-phase, by contrast to NbC, are deformable during creep at 1023 K. This means that despite the approximately tenfold increase in second-phase volume fraction associated with the NbC to G-phase transformation, material heat-treated at 1023 K so as to contain only G-phase creeps faster at a given stress. In the as-annealed condition (3.6 ksec at 1203 K), therefore, the present alloy undergoes softening *during* creep testing at the transformation of intergranular particles proceeds at 1023 K. The extent of the softening increases as the stress decreases (because the tests increase in duration).

3. Comparison of the creep rates and microstructures of 1023 and 1123 K pre-aged specimens indicates that when all the intergranular particles are G-phase then a slower creep rate results from a coarser particle distribution. This is again consistent with the deformability of G-phase particles. The latter are incoherent,

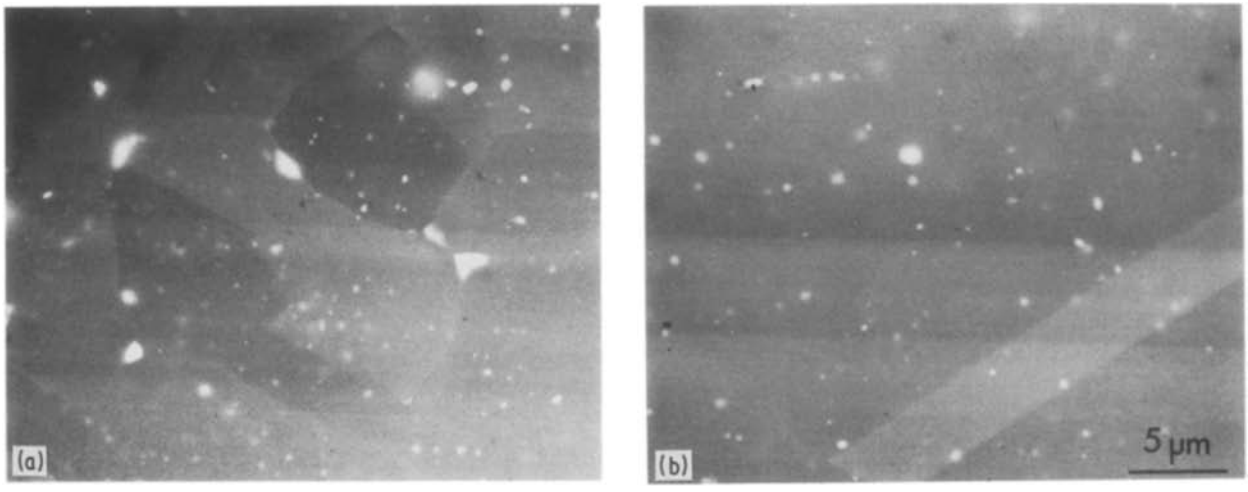

Figure 17 BSE images of (a) the present alloy (cf. Fig. 3), (b) the Ecob and Gilmour alloy, after ageing for 1.01 Msec at 1203 K, showing the finer distribution of matrix NbC particles in the former. The large intergranular particles there are of G-phase.

however, and therefore cannot in general be classically "cut" by dislocations on slip planes which are continuous across the particle–matrix interface. Glissile dislocations are therefore expected to become pinned in that interface: the particle-size dependence of the creep rate is then suggested to be associated with the rate at which the dislocations can escape.

4. The deformability of G-phase means that its formation, even as extensive grain-boundary precipitates, has little effect on creep ductility because it can plastically relax the intergranular compatibility stresses. The increase in particle volume fraction associated with the NbC to G-phase transformation may also act to suppress the deteriorations in ductility associated with secondary recrystallization.

5. It is finally to be noted that the present discussion of the effects of G-phase formation on creep behaviour at 1023 K may not be applicable to that at lower temperature. It would be expected that a significant strengthening effect would result under conditions such that the G-phase particles were undeformable.

Acknowledgements

The authors are grateful to Dr D. A. Miller for providing samples of the material studied by Powell and co-workers. This paper is published by permission of the Central Electricity Generating Board.

References

1. R. C. LOBB, to be published.
2. D. J. POWELL, PhD thesis, University of Manchester (1985).
3. A. E. DWIGHT, R. A. CONNOR and J. W. DOWNEY, *Nature* (1963) 587.
4. K. C. RUSSELL, *Prog. Mater. Sci.* **28** (1984) 229.
5. D. J. POWELL, R. PILKINGTON and D. A. MILLER, SWR/SSD/0656/R/85 CEGB Internal Document.
6. J. W. STEEDS, in "Introduction to Analytical Electron Microscopy", edited by Hren, Joy and Goldstein (Plenum, 1979).
7. R. C. ECOB and T. C. GILMOUR, to be published.
8. L. M. BROWN and R. K. HAM, in "Strengthening Methods in Crystals", edited by A. Kelly and R. B. Nicholson (Elsevier, Barking, UK, 1971).
9. R. C. ECOB, *Acta Metall.* **34** (1986) 257.
10. D. L. YANEY, J. C. GIBELING and W. D. NIX, in Proceedings of 7th International Conference on Strength of Metals and Alloys, Montreal, 1985, edited by H. J. McQueen *et al.* (Pergamon, 1986) p. 887.

Received 19 September
and accepted 8 December 1986